Analytica Chimica Acta 1324 (2024) 343040

Contents lists available at ScienceDirect

Analytica Chimica Acta

journal homepage: www.elsevier.com/locate/aca

An electrochemiluminescent imaging strategy based on CRISPR/Cas12a for ultrasensitive detection of nucleic acid

Sijian Luo [a,b], Jie Wu [b], Min Zhong [a,b], Jun Sun [b], Hang Ao [b], Xu Cao [b], Jinbo Liu [a,**], Huangxian Ju [b,*]

[a] Department of Laboratory Medicine, The Affiliated Hospital of Southwest Medical University, Sichuan Province Engineering Technology Research Center of Molecular Diagnosis of Clinical Diseases, Molecular Diagnosis of Clinical Diseases Key Laboratory of Luzhou, Luzhou, 646000, Sichuan, China
[b] State Key Laboratory of Analytical Chemistry for Life Science, School of Chemistry and Chemical Engineering, Nanjing University, Nanjing, 210023, China

HIGHLIGHTS

- A target activated Cas12a ECL imaging biosensing platform was constructed for quantitative nucleic acid detection.
- The ECL imaging method demonstrated rapid, sensitive, and specific detection of HPV-18 DNA.
- The proposed method can be conveniently used for ECL detection of multiple targets.
- This work advanced the use of ECL imaging in biomedical research.

GRAPHICAL ABSTRACT

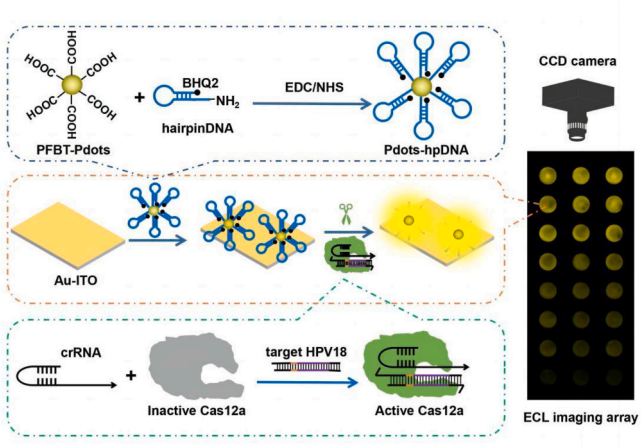

ARTICLE INFO

Handling Editor: Prof Lin Yuehe

Keywords:
Electrochemiluminescent imaging
Biosensor array
CRISPR/Cas12a
Polymer dots
HPV-18

ABSTRACT

Background: Persistent infection with human papillomavirus (HPV) significantly contributes to the development of cervical cancer. Thus, it is urgent to develop rapid and accurate methods for HPV detection. Herein, we present an ultrasensitive CRISPR/Cas12a-based electrochemiluminescent (ECL) imaging technique for the detection of HPV-18 DNA.
Result: The ECL DNA sensor array is constructed by applying black hole quencher (BHQ) and polymer dots (Pdots) co-labeled hairpin DNA (hpDNA) onto a gold-coated indium tin oxide slide (Au-ITO). The ECL imaging method involves an incubation process of target HPV-18 with a mixture of crRNA and Cas12a to activate Cas12a, followed by an incubation of the active Cas12a with the ECL sensor. This interaction causes the indiscriminate cleavage of BHQ from Pdots by digesting hpDNA on the sensor surface, leading to the restoration of the ECL

* Corresponding author.
** Corresponding author.
E-mail addresses: liujb7203@swmu.edu.cn (J. Liu), hxju@nju.edu.cn (H. Ju).

https://doi.org/10.1016/j.aca.2024.343040
Received 3 May 2024; Received in revised form 7 July 2024; Accepted 30 July 2024
Available online 31 July 2024

signal of Pdots. The ECL brightness readout demonstrates superior performance of the ECL imaging technique, with a linear detection range of 10 fM–500 pM and a limit-of-detection (LOD) of 5.3 fM.
Significance: The Cas12a-based ECL imaging approach offers high sensitivity and a broad detection range, making it highly promising for nucleic acid detection applications.

1. Introduction

Cervical cancer ranks as the fourth most prevalent cancer among women and represents a considerable risk to women's well-being. Human papillomavirus (HPV) infection typically exhibits no symptoms [1] and stands as a pivotal cause of cervical carcinogenesis [2,3]. As two of the most common high-risk HPVs, HPV-16 and HPV-18 are associated with 70 % of cancers caused by HPV infection. Hence, early HPV testing plays a vital role in screening, diagnosis, therapy, and prognosis of cervical cancer [4–6]. At present, polymerase chain reaction (PCR) serves as the gold standard for detecting HPV DNA due to its high sensitivity and specificity [7]. However, PCR's drawbacks, such as complex instrumentation, labor-intensive processes, contamination risks, and potential false-positive results, hinder its widespread use in cervical cancer screening [8]. Therefore, it is imperative to establish novel HPV DNA detection methods with good specificity, high sensitivity, low cost, and acceptable accuracy.

Clustered-regularly-interspaced-short-palindromic-repeats (CRISPR) and CRISPR-associated (Cas) proteins are essential components of archaea and bacteria's adaptive immune system. They target foreign nucleic acids and degrade them using RNA-guided programmable endonucleases [9–12]. Guided by CRISPR RNA (crRNA) hybridizing to a complementary sequence of target RNA or DNA, Cas proteins, such as the Cas9 (type II) and Cas12 (type V) families, recognize and cleave nucleic acids with high specificity. Thus, CRISPR/Cas systems serve as transformative tools for genome editing in molecular biology, genetics, and genomics fields [13,14]. LbCpf1, also known as CRISPR/Cas12a and a type V-A CRISPR-associated enzyme, exhibits unique DNase activity when activated by single-stranded or double-stranded targets. It can non-specifically cleave single-stranded DNA (*trans*-cleavage activity). This distinctive *trans*-cleavage property expands Cas12a applications from genome editing to biosensing [15–18]. Coupled with CRISPR/Cas12a's *trans*-cleavage function, various signal readouts, including electrochemiluminescence (ECL), electrochemistry, fluorescence, and color, have been used to design biosensing platforms for nucleic acids detection [19–24]. These studies demonstrate the promising potential of Cas12a-mediated biosensing in transforming nucleic acid testing protocols and implementing point-of-care diagnostic solutions.

ECL readout combines the benefits of chemiluminescence (CL) and electrochemical technology [25–27], and offers advantages such as low background interference, high sensitivity, a wide dynamic range, good controllability, and stability [28–31]. Consequently, it has emerged as a versatile and powerful analytical technique for sensing, imaging, and single-cell analysis [32–34]. ECL imaging, a nascent visualization technique utilizing electron-multiplying coupled device (EMCCD) cameras for signal acquisition, has made significant progress in single-particle analysis [35–37], multi-target detection, and cellular imaging due to its spatially and temporally resolved features and high-throughput capabilities [38,39]. To address the limitations of conventional luminescent nanomaterials, such as high bio-toxicity, low water solubility, and challenging modification [40,41], polymer dots (Pdots) have been rapidly developed and deployed in sensing and imaging detection [42–44].

This work established a CRISPR/Cas12a-based ECL imaging platform for HPV-18 DNA detection, employing poly [(9,9-dioctylfuorenyl-2,7-diyl)-*alt*-co-(1,4-benzo-{2,1′,3}-thiadiazole)] (PFBT) Pdots as biocompatible ECL nanoluminescent markers to achieve ECL signal transition [45,46]. Gold sputtered indium tin oxide slides (Au/ITO) served as substrates for constructing a nucleic acid sensing array. BHQ2-tagged aminated hairpin DNA (NH_2-hpDNA-BHQ2) was immobilized on the PFBT Pdots' surface to quench emission. The specific target recognition mechanism and *trans*-cleavage activity of Cas12a enhanced assay specificity and facilitated signal amplification. Upon the presence of target HPV-18 DNA, Cas12a was activated using its two-part recognition system, resulting in nonspecific *trans*-cleavage of the loop domain of BHQ2-labeled hpDNA. This process restored the ECL emission of PFBT Pdots, leading to significantly amplified "off-on" signals for robust ECL imaging of HPV-18 DNA (Scheme 1). The superior performance of our

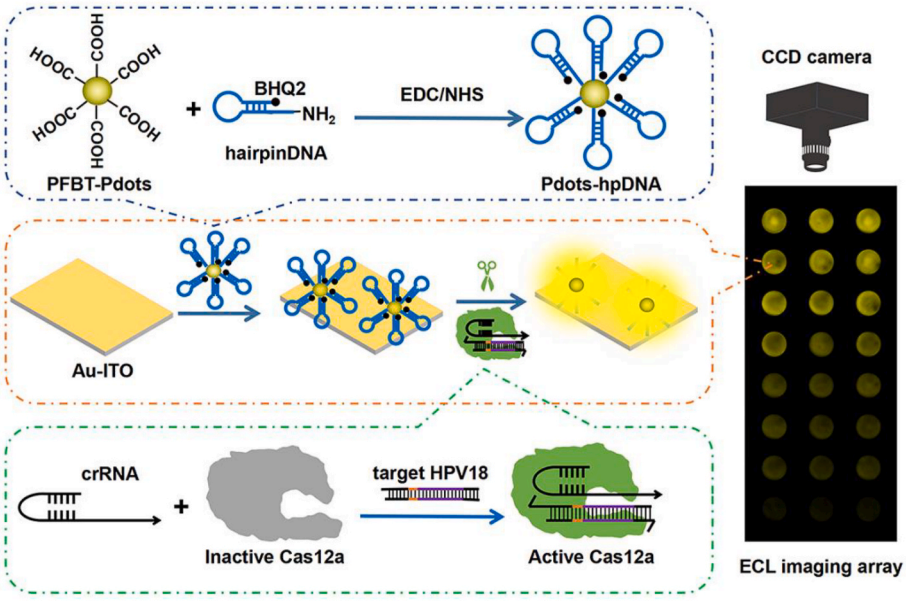

Scheme 1. Schematic illustration of the Cas12a-ECL imaging for HPV-18 detection.

Table 1
Nucleic acid sequences (from 5′ to 3′) used in this study.

Sequence name	Sequence
HPV18-TS	**TGTGTAGAAGCACATATTGT***TAAA*
HPV18-NTS	*TTTA***ACAATATGTGCTTCTACACA**
HPV16-TS	GTGCTGCCATATCTACTTCAGAAA
HPV16-NTS	TTTCTGAAGTAGATATGGCAGCAC
HPV31-TS	AGCAGTAAAATCCATAGCTCCAAA
HPV31-NTS	TTTGGAGCTATGGATTTTACTGCT
HPV33-TS	GAACTACAGTGCGTGGAATGCAAA
HPV33-NTS	TTTGCATTCCACGCACTGTAGTTC
HPV35-TS	GGTCGGTGTATGTCCTGTTGGAAA
HPV35-NTS	TTTCCAACAGGACATACACCGACC
FAM-hairpinDNA	FAM-TTTTTTCCACCACATTGAAATTGCACTATAGGAAGAGATTTACGAGGCGGTGGTGG-BHQ1
NH_2-hairpinDNA	NH_2-TTTTTTCCACCACATTGAAATTGCACTATAGGAAGAGATTTACGAGGCGGTGGTGG-BHQ2
$crRNA_{HPV18}$	UAAUUUCUACUAAGUGUAGAU***ACAAUAUGUGCUUCUACACA***

proposed ECL imaging array, coupled with CRISPR/Cas12a amplification, for HPV-18 DNA assay underscores its potential application in nucleic acid-based molecular diagnostics.

2. Experiments

2.1. Reagents and apparatus

Tetrahydrofuran (THF), tri-n-propylamine (TPrA), poly (styrene-*co*-maleic anhydride) (PSMA), 4-(2-hydroxyethyl)-1-piperazineethanesulfonic acid (HEPES) and polyethylene glycol (PEG) were purchased from Sigma-Aldrich (Shanghai, China). N-hydroxysuccinimide (NHS), 1-Ethyl-3-(3-dimethylaminopropyl) carbodiimide (EDC) and PFBT were obtained from J&K Scientific Co., Ltd. (Shanghai, China). Lba Cas12a nuclease and the corresponding 10 × buffer II were purchased from Novoprotein Scientific, Inc. (Shanghai, China). Ultrapure water was prepared using the Millipore water purification system, and RNA-related experimental manipulations were all performed in RNase-free environment. Phosphate-buffered saline (PBS, 0.1 M, pH = 7.4) were supplied by Sangon Bioengineering (Shanghai, China). The oligonucleotides employed in this work were synthesized by Sangon Bioengineering, and the sequences were listed in Table 1.

TS and NTS denote the target and non-target strands, respectively. The hybridized TS/NTS functions as the Cas12a/crRNA targeting double-stranded DNA, with the italicized segment indicating the PAM sequence. The spacer sequence of crRNA is in bold italicized. The spacer sequences of crRNA templates are in bold.

An Atomic Force Microscopic (AFM) image was captured using a Bruker atomic force microscope from Germany. Dynamic Light Scattering (DLS) analysis was conducted utilizing a 90 Plus/BI-MAS device from Brookhaven, USA. Zeta-potential analysis was carried out using a Zetasizer Nano-Z laser particle analyzer from Malvern, UK. UV Absorption Spectra were acquired using a UV-3600 UV-VIS-NIR spectrophotometer from Shimadzu, Japan. Fluorescence measurement was conducted on an F-7000 fluorescence spectrophotometer from Hitachi, Japan. Electrochemiluminescence (ECL) measurement was conducted on an MPI-A ECL analyzer from Xi'an Ramex, China. The ECL potential curve was generated using 0.1 M PBS electrolyte containing 0.1 M KNO_3 and 40 mM TPrA. The photomultiplier tube (PMT) voltage was set to 500 V, and the working potential was scanned from 0 V to +1.5 V (vs. Ag/AgCl) at 100 mV/s. ECL imaging was performed using a custom-made ECL imaging system equipped with a focus lens (EF 50 mm f/1.2 L USM, Canon, Japan) and an ultrasensitive scientific CCD camera (ANDOR iXon Ultra 897, UK) in a dark box.

2.2. Synthesis of PFBT Pdots and Pdots-hpDNA

PFBT Pdots were synthesized from a combination of PFBT and PSMA using nanoprecipitation. Initially, a solution containing 10 μg/mL PSMA and 50 μg/mL PFBT in 10 mL of THF was prepared. After 20 min of sonication and degassing, the mixture was rapidly added to 100 mL of ultrapure water and sonicated for 5 min. Subsequently, the THF solvent and water were removed by vacuum rotary evaporation, and the solution was filtered through a polyethersulfone syringe filter (pore size = 0.22 μm) to obtain a concentrated carboxyl PFBT Pdots dispersion solution.

The PFBT Pdots were functionalized with hairpin DNA (hpDNA) using an EDC/NHS-catalyzed reaction between the carboxyl group on PFBT Pdots and the amine group of hpDNA. Initially, HEPES buffer solution (1 M, 12 μL), PEG (5 % w/v, 12 μL), and PFBT Pdots dispersion solution (0.2 mg/mL, 600 μL) were thoroughly mixed, and the pH of the mixture was adjusted to 7.1 using NaOH (0.1 M). Subsequently, the mixture was added with freshly prepared EDC (10 mg/mL, 12 μL), hairpin DNA (100 μM, 40 μL), and NHS (10 mg/mL, 3 μL), followed by stirring at low speed for 24 h at room temperature using magnetic beads. The Pdots-hpDNA probe resulting from the covalent ligation reaction was ultrafiltrated eight times to eliminate free hpDNA. Lastly, the purified Pdots-hpDNA conjugate was kept at 4 °C.

2.3. Construction of ECL DNA sensors array

Firstly, Au/ITO slides were prepared using vacuum magnetron sputtering technology, resulting in a 5 nm chrome and 50 nm gold coating on the surface of the ITO slides. Subsequently, a 3 × 8 porous sticker array was affixed as the working electrode array. Finally, 2 μL of Pdots-hpDNA (50 μg/mL) was deposited onto the electrodes of each well by physical adsorption and incubated for 30 min at 37 °C to generate the nucleic acid sensor array for the proposed ECL imaging, which ensured the long-term stability.

2.4. Establishment of the CRISPR/Cas12a system and ECL imaging assay

Two complementary HPV-18 single-stranded DNAs were heated for 5 min at 95 °C and then gradually cooled to room temperature, resulting in the formation of 1.0 μM HPV-18 double-stranded DNA. Simultaneously, Cas12a was combined with $crRNA_{HPV-18}$ at a 1:2 ratio in Cas buffer and incubated for 10 min at 37 °C to form a Cas12a/crRNA functional complex. Following this, 1 μL of target HPV-18 dsDNA at various concentrations was added to 19 μL of the prepared Cas12a/crRNA mixture. Subsequently, 2 μL of these mixtures were added to each well of the sensor array and incubated for 40 min at 37 °C to digest the hpDNA, followed by washing with PBS buffer. ECL imaging was conducted at +1.5 V for 2 s in an electrolyte solution consisting of 0.1 M KNO_3, 40 mM TPrA, and 0.1 M PBS (pH = 7.4). Due to the incomplete homogeneity of Pdots-hpDNA film thickness, image J was employed to analyze the imaging brightness.

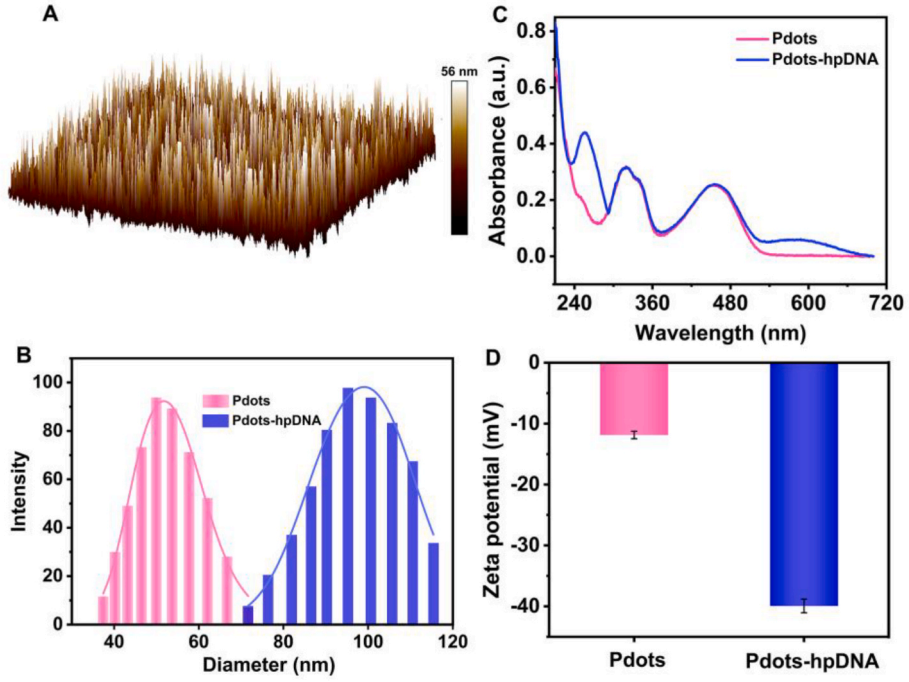

Fig. 1. (A) AFM image of PFBT Pdots. (B) DLS characterization, (C) UV absorption spectra, and (D) Zeta-potential analysis of PFBT Pdots and Pdots-hpDNA ($n = 3$).

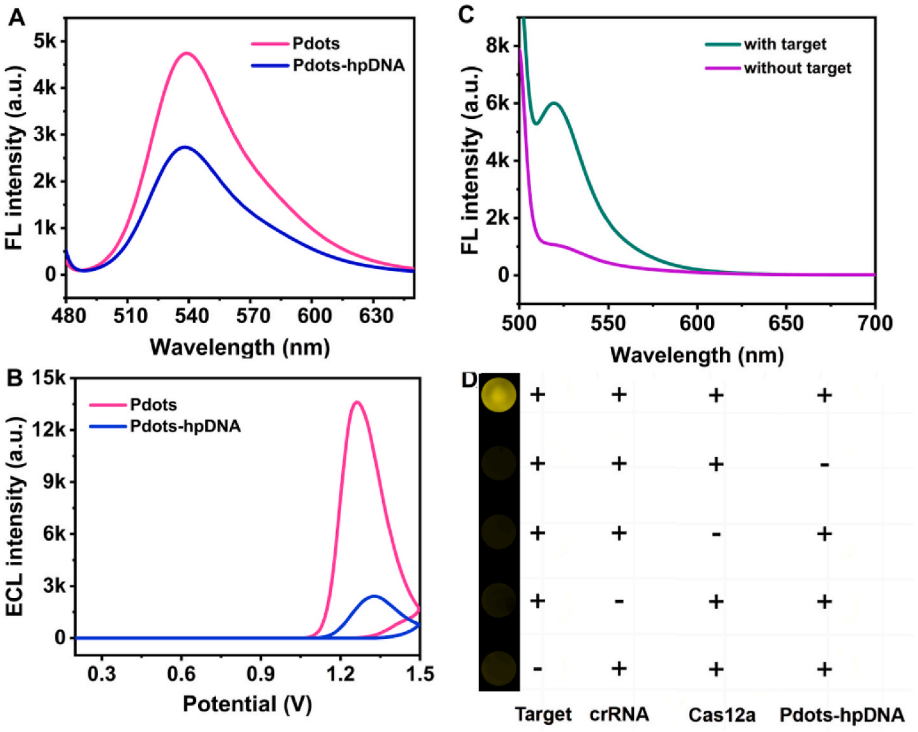

Fig. 2. (A) Fluorescent spectra, and (B) ECL potential curves of PFBT Pdots and Pdots-hpDNA. (C) Fluorescent spectra of FAM-hpDNA-BHQ1 and CRISPR/Cas12a mixture in absence and presence of targets after incubation at 37 °C for 40 min. (D) ECL images of sensor array with different detection procedures ("+" presence, "-" absence).

3. Results and discussion

3.1. Characterization of Pdots and Pdots-hpDNA

The morphological features of the prepared PFBT Pdots were characterized by AFM, which revealed spherical PFBT Pdots with a height of 56 nm (Fig. 1A). DLS measurement of PFBT Pdots indicated a hydrodynamic diameter of 59 nm, which was consistent with the AFM result, and slightly different from previous report due to the different amount of used precursor polymer [42]. Upon conjugation of hpDNA to the Pdots, there was a notable increase in hydrodynamic diameter (Fig. 1B). The Pdots-hpDNA complex exhibited 3 absorption peaks at 255, 323, and

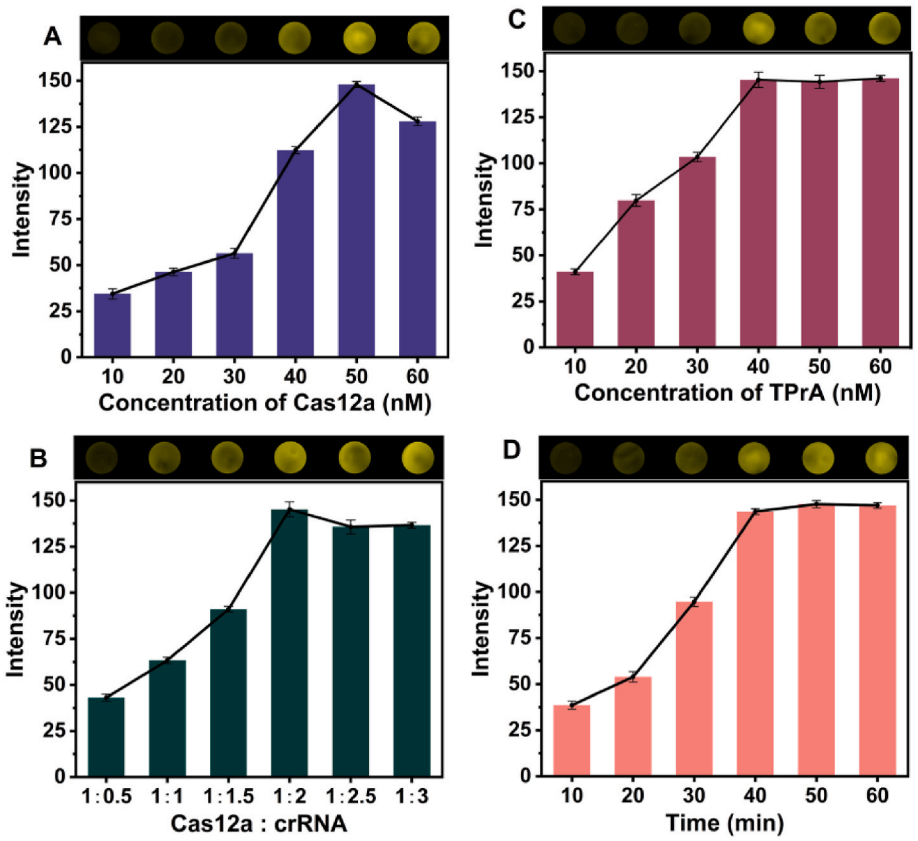

Fig. 3. Experimental parameter optimization. (A) Cas12a concentration, (B) Cas12a to crRNA concentration ratio, (C) TPrA concentration, and (D) Cleavage time of Cas12a on hpDNA-BHQ. Error bar denotes the SD from 3 repeated measurements.

453 nm subsequent to functionalization with NH_2-hpDNA. The absorption peaks at 323 nm and 453 nm aligned with those of PFBT Pdots, whereas the absorption peak at 256 nm represented a combination of PFBT Pdots with NH_2-hpDNA (Fig. 1C), indicating successful conjugation of NH_2-hpDNA to the surface of Pdots. The zeta potential values of PFBT Pdots and Pdots-hpDNA were determined to be −11.9 mV and −39.9 mV, respectively (Fig. 1D), indicating the successful conjugation of hpDNA to Pdots.

The fluorescent spectrum of Pdots-hpDNA exhibited resonance energy transfer, resulting in lower fluorescent intensity compared to Pdots at an equivalent concentration (Fig. 2A). The incorporation of BHQ2-labeled hpDNA led to an 81.7 % reduction in the ECL intensity of

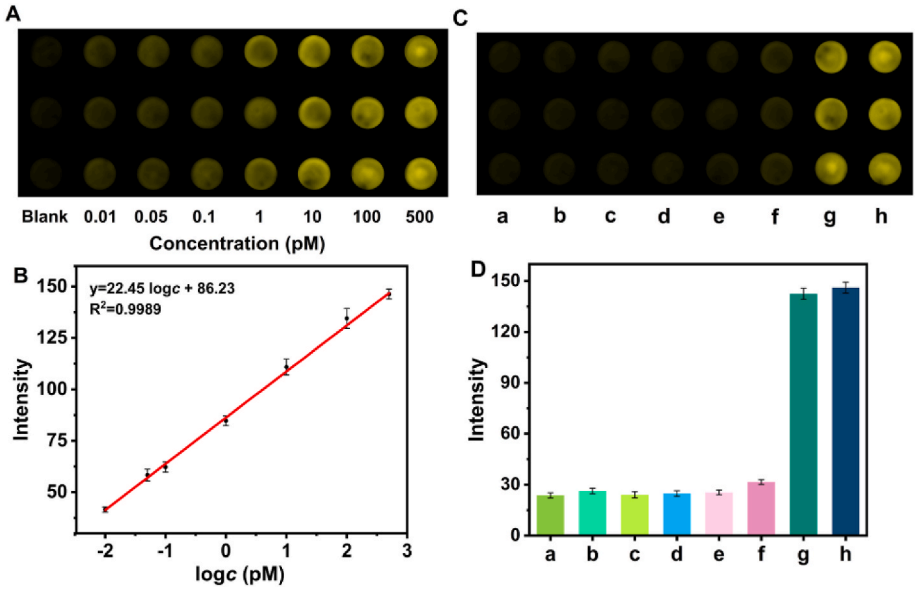

Fig. 4. (A) ECL image of HPV-18 DNA at 0, 0.01, 0.5, 0.1, 1, 10, 100, and 500 pM. (B) Calibration curve for the detection of HPV-18. (C) ECL image and (D) intensity of blank (a), HPV-16 (b), -31 (c), -33 (d), -35 (e), mixture of HPV-16/-31/-33/-35 (f), mixture of HPV-18/-16/-31/-33/HPV-35 (g), and HPV-18 (h). Error bar denotes the SD from 3 repeated measurements.

Table 2
Analytical performance evaluation of diverse biosensors for HPV detection.

Detection method	Detection time	Linear range	LOD	Reference
Electrochemiluminescence	75 min	1 pM - 10 nM	0.48 pM	[47]
Electrochemiluminescence	240 min	10 fM - 15 pM	7.6 fM	[48]
Electrochemistry	80 min	10 pM - 100 nM	3.22 pM	[49]
Electrochemiluminescence	120 min	100 pM - 200 nM	30 pM	[50]
Electrochemistry	120 min	100 fM - 100 pM	100 fM	[51]
This study	50 min	10 fM - 500 pM	5.3 fM	

PFBT Pdots (Fig. 2B) via the charge transfer between BHQ2 and excited Pdots. Hence, the proposed Pdots-hpDNA system exhibited low background for ECL imaging detection.

3.2. Feasibility of the signaling switch

Fluorescence spectroscopy was employed to assess the functionality of the designed Pdots-hpDNA as a signaling switch. In the presence of target HPV-18 dsDNA within the CRISPR/Cas12a mixture, the FAM-labeled hpDNA-BHQ underwent digestion, resulting in a 5.8 fold recovery of FAM fluorescence intensity (Fig. 2C). ECL emissions were notably pronounced when the target HPV-18 DNA (500 pM), Cas12a, crRNA, and Pdots-hpDNA were all present in the solution (Fig. 2D). Conversely, any absence of these components resulted in very weak or negligible ECL emissions, underscoring the feasibility of ECL imaging for HPV-18 DNA detection through the utilization of target-activated Cas12a and a Pdots-hpDNA film.

3.3. Optimization of experimental conditions

To achieve optimal performance of the biosensing strategy, various experimental parameters were optimized, including the Cas12a concentration, the ratio of Cas12a to crRNA, the concentration of the co-reactant (TPrA), and the *trans*-cleavage time of hpDNA-BHQ, while examining ECL brightness as the detection signal at 500 pM target DNA. The combination of crRNA and Cas12a was crucial for capturing HPV18 DNA and initiating *trans*-cleaving activity. Initially, the concentration of Cas12a was optimized, revealing maximum ECL brightness at 50 nM (Fig. 3A). Therefore, 50 nM was selected. Additionally, the concentration ratio of Cas12a to crRNA was optimized to be 1:2 (Fig. 3B). The presence of co-reactant significantly enhanced the luminescence efficiency of luminescent moieties and the sensitivity of ECL biosensors. ECL imaging signal increased steadily with increasing TPrA concentration, peaking at 40 mM, which was chosen for optimal ECL imaging detection (Fig. 3C). Furthermore, the *trans*-cleavage time of Cas12a on hpDNA-BHQ greatly influenced the performance of the Cas12a-based ECL imaging biosensor, optimized between 10 min and 60 min. As depicted in Fig. 3D, the ECL signal exhibited a rapid surge prior to the 40-min mark, followed by a modest incline. To ensure the timeliness of the Cas12a-based ECL biosensor, the optimal *trans*-cleavage time of hpDNA-BHQ by active Cas12a was determined to be 40 min.

Table 3
HPV-18 detection in serum specimens.

Specimen number	Added (fM)	Found (fM)	Recovery (%)	RSD (%) (n = 3)
1	10	11.2	112	4.67
2	100	105.9	105.9	3.77
3	1000	999.4	99.94	2.46
4	10,000	9925.3	99.25	2.52

3.4. ECL imaging biosensing performance for detection of HPV-18

Under optimized conditions, the Pdots-hpDNA-based sensor array was employed for ECL imaging measurements. To assess the sensitivity and linear range of the CRISPR ECL biosensor for HPV-18 DNA quantification, various concentrations of HPV-18 DNA ranging from 10 fM to 500 pM were tested. The ECL brightness enhanced proportionally with HPV-18 DNA concentrations (Fig. 4A). Graphs depicting the integrated ECL intensity derived from the designated region exhibited excellent linearity when plotted against the logarithm of HPV-18 DNA concentration, with a linear equation of $I = 22.45 \lg c + 86.23$ ($R^2 = 0.9989$) and a limit-of-detection (LOD) of 5.3 fM (Fig. 4B). Compared to other published HPV sensing techniques, the proposed ECL imaging strategy demonstrated a lower LOD, broader detection range, and shorter reaction time for quantifying HPV DNA (Table 2).

The selectivity of the proposed biosensor was assessed by comparing the ECL responses of DNA interferents with various sequences from common HPV subtypes, including HPV-16, -31, -33, and -35. Each interfering sequence was present at a concentration of 50 nM, which was 100 times higher than that of the target HPV-18 (500 pM). As anticipated, these interferents, either individually or in a mixture, exhibited the same signal as the blank (Fig. 4C). However, the mixture containing HPV-18 along with HPV-31, -33, -35, and -16 displayed a response identical to that of HPV-18 alone (Fig. 4D). This observation suggests minimal interference from these sequences on target detection, thereby confirming the excellent selectivity of the biosensing strategy. Such high specificity may be due to the excellent recognition capability of the CRISPR/Cas12a system.

3.5. Detection of HPV-18 in serum specimens

To assess the anti-interference and detection efficiency of the proposed ECL imaging strategy in complex biological fluids, recovery tests were conducted by adding varying amounts of HPV18 DNA to undiluted human serum samples. Table 3 demonstrates the recovery rates ranging from 99.25 % to 112 % in human serum samples. The relative standard deviation (RSD) fell within the range of 2.46 %–4.67 %, indicating promising prospects for clinical sample detection using the presented ECL imaging biosensors.

4. Conclusion

This study introduces a CRISPR/Cas12a-based ECL imaging strategy for highly sensitive nucleic acid detection without the need for target pre-amplification. Benefiting from the highly efficient ECL emission of PFBT Pdots and the *trans*-cleavage capability of the Cas12a system, this strategy exhibits strong selectivity, excellent accuracy, acceptable precision, and high sensitivity for detecting target HPV-18 DNA, with a LOD of 5.3 fM. More importantly, this method can be conveniently applied for the detection of multiple targets through ECL imaging of nucleic acid

arrays. Hence, this strategy holds promising potential as a universal approach for detecting pathogen nucleic acids, providing more precise data and evaluation recommendations for clinical disease diagnosis.

CRediT authorship contribution statement

Sijian Luo: Writing – original draft, Investigation, Formal analysis, Data curation, Conceptualization. **Jie Wu:** Investigation, Formal analysis, Conceptualization. **Min Zhong:** Investigation, Formal analysis. **Jun Sun:** Investigation, Formal analysis. **Hang Ao:** Investigation, Formal analysis. **Xu Cao:** Investigation, Formal analysis. **Jinbo Liu:** Writing – review & editing, Supervision, Conceptualization. **Huangxian Ju:** Writing – review & editing, Supervision, Project administration, Funding acquisition.

Declaration of competing interest

The authors declare that they have no known competing financial interests or personal relationships that could have appeared to influence the work reported in this paper.

Data availability

No data was used for the research described in the article.

Acknowledgements

This research was financially supported by the National Natural Science Foundation of China (21890741, 21827812), the Science and Technology Project of Nanjing City (202110023) and the Science and Technology Project of Southwest Medical University (2022QN022, 2022QN119).

References

[1] L.E. Markowitz, E.R. Unger, Human papillomavirus vaccination, N. Engl. J. Med. 388 (2023) 1790–1798.
[2] L. Rahangdale, C. Mungo, S. O'Connor, C.J. Chibwesha, N.T. Brewer, Human papillomavirus vaccination and cervical cancer risk, BMJ 379 (2022) e070115.
[3] X.H. Yang, Y.Y. Li, Y. Tang, Z.Y. Li, S.F. Wang, X. Luo, T.W. He, A.H. Yin, M.Y. Luo, Cervical HPV infection in Guangzhou, China: an epidemiological study of 198,111 women from 2015 to 2021, Emerg. Microb. Infect. 12 (2023) e2176009.
[4] J.Y. Lei, L.S. Arroyo-Mühr, C. Lagheden, C. Eklund, S.N. Kleppe, M. Elfström, B. Andrae, P. Sparén, J. Dillner, K. Sundström, Human papillomavirus infection determines prognosis in cervical cancer, J. Clin. Oncol. 40 (2022) 1522–1528.
[5] R. van den Helder, R.D.M. Steenbergen, A.P. van Splunter, C.H. Mom, M.Y. Tjiong, I. Martin, F.M.F. Rosier-van Dunné, I.A.M. van der Avoort, M.C.G. Bleeker, N.E. van Trommel, HPV and DNA methylation testing in urine for cervical intraepithelial neoplasia and cervical cancer detection, Clin. Cancer Res. 28 (2022) 2061–2068.
[6] M. Safaeian, T.C.J. Wright, M.H. Stoler, J. Ranger-Moore, S. Rehm, S. Aslam, Q. J. Fang, P. Volkir, R. Ridder, The improving primary screening and colposcopy triage trial: human papillomavirus, cervical cytology, and histopathologic results from the baseline and 1-year follow-up phase, Am. J. Obstet. Gynecol. 225 (2021) 278.e1–278.e16.
[7] F.L.S.G. Santos, M.C.V. Invenção, E.D. Araújo, G.S. Barros, M.V. A Batista, Comparative analysis of different PCR-based strategies for HPV detection and genotyping from cervical samples, J. Med. Virol. 93 (2021) 6347–6354.
[8] K. Alfaro, M. Maza, M. Cremer, R. Masch, M. Soler, Removing global barriers to cervical cancer prevention and moving towards elimination, Nat. Rev. Cancer 21 (2021) 607–608.
[9] R. Sorek, V. Kunin, P. Hugenholtz, CRISPR–a widespread system that provides acquired resistance against phages in bacteria and archaea, Nat. Rev. Microbiol. 6 (2008) 181–186.
[10] Z.Y. Weng, Z. You, J. Yang, N. Mohammad, M.S. Lin, Q.S. Wei, X. Gao, Y. Zhang, CRISPR-Cas biochemistry and CRISPR-based molecular diagnostics, Angew. Chem. t Ed. 62 (2023) e202214987.
[11] S.P.B. van Beljouw, J. Sanders, A. Rodríguez-Molina, S.J.J. Brouns, RNA-targeting CRISPR-Cas systems, Nat. Rev. Microbiol. 21 (2023) 21–34.
[12] J.Y. Wang, J.A. Doudna, CRISPR technology: a decade of genome editing is only the beginning, Science 379 (2023) eadd8643.
[13] J.Y. Wang, P. Pausch, J.A. Doudna, Structural biology of CRISPR-Cas immunity and genome editing enzymes, Nat. Rev. Microbiol. 20 (2022) 641–656.
[14] P. Pausch, K.M. Soczek, D.A. Herbst, C.A. Tsuchida, B. Al-Shayeb, J.F. Banfield, E. Nogales, J.A. Doudna, DNA interference states of the hypercompact CRISPR-CasΦ effector, Nat. Struct. Mol. Biol. 28 (2021) 652–661.
[15] J.S. Chen, E.B. Ma, L.B. Harrington, M. Da Costa, X.R. Tian, J.M. Palefsky, J. A. Doudna, CRISPR-Cas12a target binding unleashes indiscriminate single-stranded DNase activity, Science 360 (2018) 436–439.
[16] H.N. Li, Y. Xie, F.M. Chen, H.W. Bai, L.S. Xiu, X.N. Zhou, X.K. Guo, Q.Q. Hu, K. Yin, Amplification-free CRISPR/Cas detection technology: challenges, strategies, and perspectives, Chem. Soc. Rev. 52 (2023) 361–382.
[17] T. Yamano, H. Nishimasu, B. Zetsche, H. Hirano, I.M. Slaymaker, Y.Q. Li, I. Fedorova, T. Nakane, K.S. Makarova, E.V. Koonin, R. Ishitani, F. Zhang, O. Nureki, Crystal structure of Cpf1 in complex with guide RNA and target DNA, Cell 165 (2016) 949–962.
[18] R.J. Fu, Y.L. Xianyu, Gold nanomaterials-implemented CRISPR-Cas systems for biosensing, Small 19 (2023) e2300057.
[19] Q. Zhao, Z. Gao, X. Liu, X. Song, D. Wu, H. Ma, X. Ren, Y. Li, Q. Wei, Dual-signal integrated aptasensor for microcystin-LR detection via in situ generation of silver nanoclusters induced by circular DNA strand displacement reactions, Anal. Chem. 95 (2023) 14317–14323.
[20] M. Zhong, J.B. Liu, J. Wu, J.Q. Li, N.N. Luo, C.L. Zhu, R. Liu, Q.F. Xia, H.X. Ju, Proximity sequence enhanced CRISPR-Cas12a connected through hybridization chain reaction for sensitive biosensing of dengue virus, Sens. Actuators. B-Chem. 366 (2022) 132011.
[21] S.J. Lin, Y.Z. Lin, J. Wu, G.M. Li, X.T. Wu, N.N. Luo, W.T. Li, C.L. Zhu, R. Liu, Q. Q. Xu, Q.F. Xia, H.X. Ju, A ratiometric fluorescent biosensor for rapid detection of Burkholderia pseudomallei by dual CRISPR/Cas12a trans-cleavage assisted signal enhancement, Sens. Actuators. B-Chem. 379 (2023) 133204.
[22] L.L. Li, S.Q. Yu, J. Wu, H.X. Ju, Regulation of target-activated CRISPR/Cas12a on surface binding of polymer dots for sensitive electrochemiluminescence DNA analysis, Anal. Chem. 95 (2023) 7396–7402.
[23] J.Y. Wang, X.L. Wang, B. Li, K. Zhang, J.Y. Mao, Entropy-driven reactions for controlling CRISPR/Cas12a and constructing an electrochemical biosensor for cardiac biomarkers detection, Microchim. Acta 190 (2023) 440–449.
[24] Y.F. Dai, R.A. Somoza, L. Wang, J.F. Welter, Y. Li, A.I. Caplan, C.C. Liu, Exploring the trans-cleavage activity of CRISPR-Cas12a (cpf1) for the development of a universal electrochemical biosensor, Angew. Chem. Int. Ed. 58 (2019) 17399–17405.
[25] H.L. Qi, C.X. Zhang, Electrogenerated chemiluminescence biosensing, Anal. Chem. 92 (2020) 524–534.
[26] B. Babamiri, D. Bahari, A. Salimi, Highly sensitive bioaffinity electrochemiluminescence sensors: recent advances and future directions, Biosens. Bioelectron. 142 (2019) 111530.
[27] X.C. Liu, S. Zhao, L.L. Tan, Y. Tan, Y. Wang, Z.Y. Ye, C.J. Hou, Y. Xu, S. Liu, G. X. Wang, Frontier and hot topics in electrochemiluminescence sensing technology based on CiteSpace bibliometric analysis, Biosens. Bioelectron. 201 (2022) 113932.
[28] S.S. Li, A.J. Wang, P.X. Yuan, L.P. Mei, L. Zhang, J.J. Feng, Heterometallic nanomaterials: activity modulation, sensing, imaging and therapy, Chem. Sci. 13 (2022) 5505–5530.
[29] W.X. Zhu, J.R. Dong, G.X. Ruan, Y. Zhou, J.D. Feng, Quantitative single-molecule electrochemiluminescence bioassay, Angew. Chem. Int. Ed. 62 (2023) e202214419.
[30] E. Sobhanie, F. Salehnia, G.B. Xu, Y. Hamidipanah, S. Arshian, A. Firoozbakhtian, M. Hosseini, M.R. Ganjali, S. Hanif, Recent trends and advancements in electrochemiluminescence biosensors for human virus detection, Trends Anal. Chem. 157 (2022) 116727.
[31] K.Q. Wu, Y.J. Zheng, R. Chen, Z.X. Zhou, S.Q. Liu, Y.F. Shen, Y.J. Zhang, Advances in electrochemiluminescence luminophores based on small organic molecules for biosensing, Biosens. Bioelectron. 223 (2023) 115031.
[32] N.N. Wang, Y.N. Feng, Y.W. Wang, H.X. Ju, F. Yan, Electrochemiluminescent imaging for multi-immunoassay sensitized by dual DNA amplification of polymer dot signal, Anal. Chem. 90 (2018) 7708–7714.
[33] Y.R. Zhao, J. Descamps, N. Al Hoda Al Bast, M. Duque, J. Esteve, B. Sepulveda, G. Loget, N. Sojic, All-optical electrochemiluminescence, J. Am. Chem. Soc. 145 (2023) 17420–17426.
[34] J. Descamps, C. Colin, G. Tessier, S. Arbault, N. Sojic, Ultrasensitive imaging of cells and sub-cellular entities by electrochemiluminescence, Angew. Chem. Int. Ed. 62 (2023) e202218574.
[35] J.J. Zhang, S. Arbault, N. Sojic, D.C. Jiang, Electrochemiluminescence imaging for bioanalysis, Annu. Rev. Anal. Chem. 12 (2019) 275–295.
[36] M.M. Chen, C.H. Xu, W. Zhao, H.Y. Chen, J.J. Xu, Single cell imaging of electrochemiluminescence-driven photodynamic therapy, Angew. Chem. Int. Ed. 61 (2022) e202117401.
[37] Y. Zhou, J.R. Dong, P.L. Zhao, J.K. Zhang, M. Zheng, J.D. Feng, Imaging of single bacteria with electrochemiluminescence microscopy, J. Am. Chem. Soc. 145 (2023) 8947–8953.
[38] N.N. Wang, L.Z. Chen, W.W. Chen, H.X. Ju, Potential- and color-resolved electrochemiluminescence of polymer dots for array imaging of multiplex microRNAs, Anal. Chem. 93 (2021) 5327–5333.
[39] H.K. Li, Q.Q. Cai, J.R. Wang, G.F. Jie, Versatile FeMoOv nanozyme bipolar electrode electrochemiluminescence biosensing and imaging platform for detection of H_2O_2 and PSA, Biosens. Bioelectron. 232 (2023) 115315.
[40] C. Wang, S.Q. Liu, H.X. Ju, Electrochemiluminescence nanoemitters for immunoassay of protein biomarkers, Bioelectrochemistry 149 (2023) 108281.
[41] A. Abdussalam, G.B. Xu, Recent advances in electrochemiluminescence luminophores, Anal. Bioanal. Chem. 414 (2022) 131–146.
[42] Y. He, X.X. Hu, Z.J. Gong, S.H. Chen, R. Yuan, A novel electrochemiluminescence biosensor based on the self-ECL emission of conjugated polymer dots for lead ion detection, Microchim. Acta 187 (2020) 237–244.

[43] J.Y. Sun, H. Mei, F. Gao, Ratiometric detection of copper ions and alkaline phosphatase activity based on semiconducting polymer dots assembled with rhodamine B hydrazide, Biosens. Bioelectron. 91 (2017) 70–75.
[44] C.T. Kuo, A.M. Thompson, M.E. Gallina, F.M. Ye, E.S. Johnson, W. Sun, M.X. Zhao, J.B. Yu, I.C. Wu, B. Fujimoto, C.C. DuFort, M.A. Carlson, S.R. Hingorani, A. L. Paguirigan, J.P. Radich, D.T. Chiu, Optical painting and fluorescence activated sorting of single adherent cells labelled with photoswitchable Pdots, Nat. Commun. 7 (2016) 11468.
[45] Y.N. Feng, F. Sun, N.N. Wang, J.P. Lei, H.X. Ju, $Ru(bpy)_3^{2+}$ incorporated luminescent polymer dots: double-enhanced electrochemiluminescence for detection of single-nucleotide polymorphism, Anal. Chem. 89 (2017) 7659–7666.
[46] J.H. Luo, Q. Li, S.H. Chen, R. Yuan, Coreactant-free dual amplified electrochemiluminescent biosensor based on conjugated polymer dots for the ultrasensitive detection of microRNA, ACS Appl. Mater. Interfaces 11 (2019) 27363–27370.
[47] P. Fliu, K.R. Zhao, Z.J. Liu, L. Wang, S.Y. Ye, G.X. Liang, Cas12a-based electrochemiluminescence biosensor for target amplification-free DNA detection, Biosens. Bioelectron. 176 (2021) 112954.
[48] Y.H. He, Y.H. Liu, L.J. Cheng, Y.Y. Yang, B. Qiu, L.H. Guo, Y. Wang, Z.Y. Lin, G. L. Hong, Highly reproducible and sensitive electrochemiluminescence biosensors for HPV detection based on bovine serum albumin carrier platforms and hyperbranched rolling circle amplification, ACS Appl. Mater. Interfaces 13 (2021) 298–305.
[49] J. Liu, Q. Wan, R.J. Zeng, D.P. Tang, An ultrasensitive homogeneous electrochemical biosensor based on CRISPR-Cas12a, Anal. Methods 13 (2021) 3227–3232.
[50] Y.X. Nie, X. Zhang, Q. Zhang, Z.H. Liang, Q. Ma, X.G. Su, A novel highly efficient electrochemiluminescence sensor based on reductive Cu(I) particles catalyzed Zn-doped MoS2 QDs for HPV 16 DNA determination, Biosens. Bioelectron. 160 (2020) 112217.
[51] J. Su, Y.Q. Ke, N. Maboyi, X. Zhi, S.J. Yan, F.W. Li, B. Zhao, X.L. Jia, S.P. Song, X. T. Ding, CRISPR/Cas12a powered DNA framework-supported electrochemical biosensing platform for ultrasensitive nucleic acid analysis, Small Methods 5 (2021) e2100935.